Most probable trajectory of a muon in a scattering medium, when input and output trajectories are known

Christopher J. Benton, Nathan D. Smith, Stephen J. Quillin, Christopher A. Steer

September 17, 2012

Abstract

Tomographic imaging using cosmic ray muons has a range of applications including homeland security and geological imaging. To this end, we have developed a technique to calculate the most probable muon trajectory through a scattering material, given its measured entry and exit trajectories. This method has the potential to improve tomographic algorithms, in particular by replacing the muon paths assumed by the Point Of Closest Approach (POCA) method, with more realistic paths. These paths can be calculated for arbitary matter distributions, rather than just the point scatterers assumed by POCA.

1 Introduction

Interactions between cosmic rays and particles in the upper atmosphere generate showers of high energy charged particles, including muons. Muons are similar to electrons, but with about 207 times the mass. Due to their high energy, in the order of GeV, cosmic ray muons are highly penetrating, and can travel through hundreds of metres of solid material, albeit with energy loss and scattering.

The scattering depends on the composition of the material, and so by observing the trajectory of a muon before and after passing though an object, information about that object's internal composition can be obtained. This property has led to the development of muon tomography, where the information obtained from many muon trajectories is used to derive a 3D image of an object's interior [1, 2]. Cosmic ray showers contain both muons and antimuons, but in the context of muon tomography, the distinction between the two is unimportant, as they are scattered by neutral matter in a very similar way.

Muon tomography is particularly promising for homeland security applications, including the detection of smuggled nuclear material [2], as high atomic-mass elements such as uranium and plutonium are very strongly scattering. Furthermore, due to the penetrating nature of the muons, it is very difficult to shield against muon tomography. This long penetration distance also enables imaging of large-scale objects, such as large industrial structures [3] and geological features [4, 5].

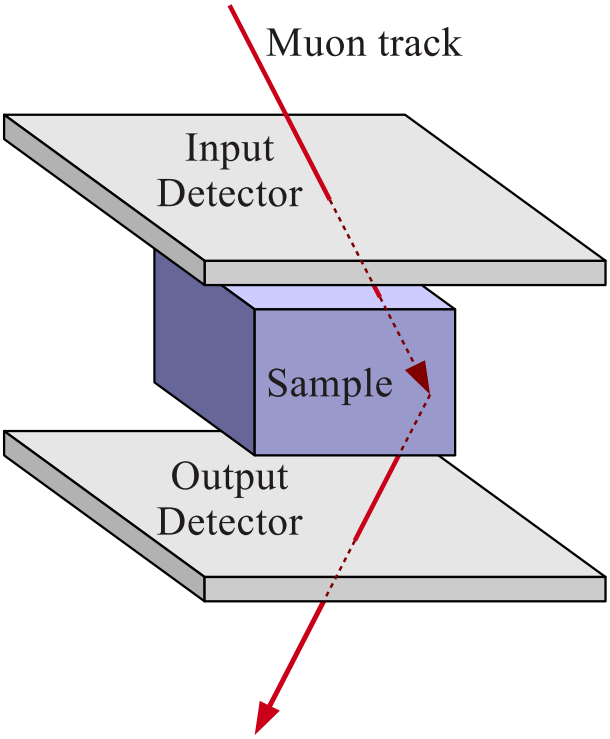

Figure 1: Schematic of a muon tomographic device. The muon path is that assumed by the point of closest approach (POCA) method. Dotted sections of the muon path are those in which the line is occluded by other objects in the diagram.

The data processing algorithms which underlie muon tomography, are still an area of active research. Current algorithms are based on the Point Of Closest Approach (POCA) model of this trajectory [6, 7, 8]. This extrapolates the ingoing trajectory of the muon in a straight line forwards, and the outgoing trajectory in a straight line backwards, and assumes that the muon is scattered from one trajectory to the other, due to a strongly scattering region at the point of closest approach. A schematic of a POCA path can be seen in Figure 1. The density of material in that region can be estimated from the angle of deflection, and by combining lots of muon measurements, a 3D image can be built up.

However, the POCA method makes certain assumptions as to the physical nature of the system, which are not necessarily true, and so may degrade the quality of the resulting images. One such problem is that in three dimensions, two lines will not necessarily intersect, and so in general, some contrivance is required to link the input and output trajectories. This can be done by assuming that the scattering region provides a translation as well as a deflection, or by tweaking the input and output trajectories so that the two intersect.

Another problem with the POCA method, is that by insisting on straight lines through most of the object, with only one bend, it presumes that the object being observed is best understood as having a single strongly scattering region, with vacuum elsewhere. The assumption is appropriate in samples containing large amounts of empty space, but it becomes unreliable for more uniform materials, such as the rock inside a mountain. As well as being unreliable, the assumption is inflexible, as there is no way of incorporating prior knowledge, and in particular, of allowing the knowledge derived from other muon events to inform the analysis of a specific event. In fact, when multiple strong scatterers are present, a POCA reconstruction can make conflicting assumptions. For example, if a region is far away from the POCA region, but still intersected by the POCA path, it will be regarded as weakly scattering, even it has been established as strongly scattering by other muon measurements.

We have succeeded in moving beyond this assumption, using a technique which amounts to the minimization of a functional describing the curvature of the trajectory, which is described in Section 2. (Somewhat similar analysis has been done for protons [9], but using different mathematical techniques.) In Section 3, a numerical method for performing this functional minimization, given a known input and

output trajectory, is described. In Section 4 the results for a variety of cases are presented. In Section 5 potential applications for the method, including improved tomographic reconstructions, are discussed.

2 Formulating path calculation as minimization of curvature functional

The probability density function (PDF) f that a muon will undergo an angular deflection of $\delta\theta$, with an azimuth relative to its path ϕ, over a small distance increment δl, is assumed to obey a Fokker-Planck equation of the form

$$\frac{\partial f}{\partial (\delta l)} = D\nabla^2 f \tag{1}$$

The diffusion coefficient D is related to the muon's momentum, and the scattering cross section of the intervening material [10]. This formulation, and the Gaussian probability distribution that results from it, is a good approximation to reality for most scattering angles. However, a Gaussian probability distribution underestimates the probability of comparatively rare wide-angle scattering events [10, 11]. Resolving this discrepancy is beyond the scope of this paper, but will be the subject of future research.

The Laplacian operator is defined in $\delta\theta$ and ϕ as

$$\nabla^2 \equiv \frac{\partial^2}{\partial (\delta\theta)^2} + \frac{\cos(\delta\theta)}{\sin(\delta\theta)} \frac{\partial}{\partial (\delta\theta)} + \frac{1}{\sin^2(\delta\theta)} \frac{\partial^2}{\partial \phi^2} \tag{2}$$

If $\delta\theta$ is small, the approximations $\sin(\delta\theta) \approx \theta$ and $\cos(\delta\theta) \approx 1$ are valid, giving

$$\frac{\partial f}{\partial (\delta l)} = D\left(\frac{\partial^2 f}{\partial (\delta\theta)^2} + \frac{1}{\delta\theta} \frac{\partial f}{\partial (\delta\theta)} + \frac{1}{(\delta\theta)^2} \frac{\partial^2 f}{\partial \phi^2} \right) \tag{3}$$

Assuming the certainty of zero deflection at zero distance, the initial condition at $\delta l = 0$ should be a 2-dimensional delta function centered at $\delta\theta = 0$. A solution that matches this condition is

$$f(\delta\theta, \delta l) = \frac{1}{4\pi D\delta l} \exp\left(-\frac{(\delta\theta)^2}{4D\delta l} \right) \tag{4}$$

where $\delta\theta \geq 0$. This solution is affected by the small angle approximation, as it lacks the 2π periodicity in $\delta\theta$ that would be present if $\delta\theta$ were a proper angle. However, the extremely wide angle scattering events that would make this discrepancy important are vanishingly improbable. A further issue is that the normalization factor in front of equation 4 assumes that $\delta\theta$ is integrated up to ∞, rather than the maximum physical value of π. However, for narrow scattering angles, the integral from π to ∞ is negligible.

Despite the fact that equation 4 only contains $\delta\theta$, it is *not* the PDF for scattering by $\delta\theta$, but the solid angle PDF for scattering by $\delta\theta$ at ϕ. The infinitesimal solid angle element is $\sin(\delta\theta)\ \mathrm{d}(\delta\theta)\ \mathrm{d}\phi$, which in the small angle approximation becomes $\delta\theta\ \mathrm{d}(\delta\theta)\ \mathrm{d}\phi$. To obtain the PDF for $\delta\theta$ alone, it is necessary to integrate over ϕ, giving

$$f'(\delta\theta, \delta l) = \int_{\phi=0}^{2\pi} \frac{1}{4\pi D\delta l} \exp\left(-\frac{(\delta\theta)^2}{4D\delta l} \right) \delta\theta\ \mathrm{d}\phi \tag{5}$$

$$= \frac{\delta\theta}{2D\delta l} \exp\left(-\frac{(\delta\theta)^2}{4D\delta l} \right) \tag{6}$$

The two PDFs are qualitatively different, as that given by equation 4 peaks at zero, while that given by equation 6 peaks at a non-zero value. The difference is due to the fact that there is only one way in which zero scattering can occur, but there are many ways in which a scattering by a particular non-zero angle can occur.

Having made the distinction, it should be noted that the solid angle PDF given by equation 4 is the correct formulation for muon tomography, as to evaluate the probability of a particular muon trajectory, it is the actual direction taken, and not just the bending angle, that is important.

The probability of a muon scattering about an angle $\delta\theta_n$ with azimuthal angle ϕ_n over a distance δl_n through a section of material with scattering coefficient D_n can be evaluated as

$$\begin{aligned} p_n &= \int_{\phi=\phi_n}^{\phi_n+\omega_\phi} \int_{\delta\theta=\delta\theta_n}^{\delta\theta_n+\omega_\theta} f\left(\delta\theta, \delta l_n\right)\ \delta\theta\ \mathrm{d}\phi\ \mathrm{d}\left(\delta\theta\right) && (7) \\ &= \left[-\frac{\omega_\phi}{2\pi}\exp\left(-\frac{\left(\delta\theta\right)^2}{4D_n\delta l_n}\right)\right]_{\delta\theta=\delta\theta_n}^{\delta\theta_n+\omega_\theta} && (8) \\ &= \exp\left(-\frac{1}{4D_n}\left(\frac{\delta\theta_n}{\delta l_n}\right)^2\delta l_n\right)\ \frac{\omega_\phi}{2\pi}\left[1-\exp\left(-\frac{\omega_\theta^2+2\omega_\theta\delta\theta_n}{4D_n\delta l_n}\right)\right] && (9) \end{aligned}$$

where ω_θ and ω_ϕ are ranges of acceptance over which $\delta\theta$ and ϕ are held to match $\delta\theta_n$ and ϕ_n. Assuming that the probability distribution for a given section of the muon path depends only on the muon position at the start of that section, then the combined probability for multiple sections is given by

$$\begin{aligned} p &= \prod_{n=1}^{N} p_n && (10) \\ &= \exp\left(-\sum_{n=1}^{N}\frac{1}{4D_n}\left(\frac{\delta\theta_n}{\delta l_n}\right)^2\delta l_n\right)\ \prod_{n=1}^{N}\lambda_n && (11) \end{aligned}$$

where the factors λ_n are given by

$$\lambda_n = \frac{\omega_\phi}{2\pi}\left[1-\exp\left(-\frac{\omega_\theta^2+2\omega_\theta\delta\theta_n}{4D_n\delta l_n}\right)\right] \quad (12)$$

A complication arises from the fact that in the continuous limit, there are an infinite number of paths that the muon can take, and so the probability of it taking any one path is formally zero. However, in terms of limiting ratios, it can still make sense to describe one path as more probable than another, and so establish a particular path as the most probable. At present, we are unsure precisely how to deal with these ratios, as when the infinitesimal limit is taken, they seem to stubbornly tend towards zero or infinity. This problem is discussed further in Section 5.

Nevertheless, it is possible to get a finite representation of the probability, by noting that equation 11 consists of a factor which tends towards a meaningful finite value in the continuous limit, multiplied by a product of the λ_n factors. These factors are always smaller than one, and so in the continuous limit, when an infinite number of them are present, the product vanishes to zero. It is mathematically possible to set all of λ_n to one, by setting ω_ϕ to 2π, and by setting ω_θ to any finite value, so that the ratio $\delta l/\omega_\theta$ becomes infinitesimal in the continuous limit. This operation, however, is physically invalid, as if ω_ϕ is 2π, then all possible azimuthal angles are regarded as conforming to the curve, and so the connection between a particular curve and the evaluated probability is broken. It is possible to retain this connection by allowing ω_ϕ to approach 2π as a limiting case. By choosing ω_ϕ and ω_θ as

$$\begin{aligned} \omega_\phi &= 2\pi\left(1-\frac{1}{N}\right)^\alpha && (13) \\ \omega_\theta &= 1 && (14) \end{aligned}$$

the product $\prod_n \lambda_n$ tends, in the infinite limit, towards a value of

$$\lim_{N\to\infty}\left(1-\frac{1}{N}\right)^{\alpha N} = e^{-\alpha} \quad (15)$$

This can be made arbitrarily small (by increasing α), and so the restriction, although infinitesimal for each element, is acting to substantially constrain the number of permitted paths. Therefore the continuous probability can be represented as

$$P = \exp\left[-\int_{l_1}^{l_2}\frac{1}{4D}\left(\frac{\mathrm{d}\theta}{\mathrm{d}l}\right)^2\mathrm{d}l-\alpha\right] \quad (16)$$

Identifying $|\mathrm{d}\theta/\mathrm{d}l|$ with the curvature κ gives

$$P = \exp\left[-\int_{l_1}^{l_2} \frac{\kappa^2}{4D}\mathrm{d}l - \alpha\right] \tag{17}$$

Equation 17 is written using an intrinsic coordinate system, which depends only on the muon's path. This demonstrates that the method is not tied to any extrinsic coordinate system, and so fully represents the 3D geometry of the situation. This differs from the approach in Ref. [9], where the scattering processes over two fixed orthogonal planes are assumed to be independent.

For most applications, it is far more convenient to use a coordinate system based around the muon detectors, rather than the muons themselves. Therefore, under the assumption that the detectors form two parallel planes, a Cartesian coordinate system was chosen, as shown in Figure 2.

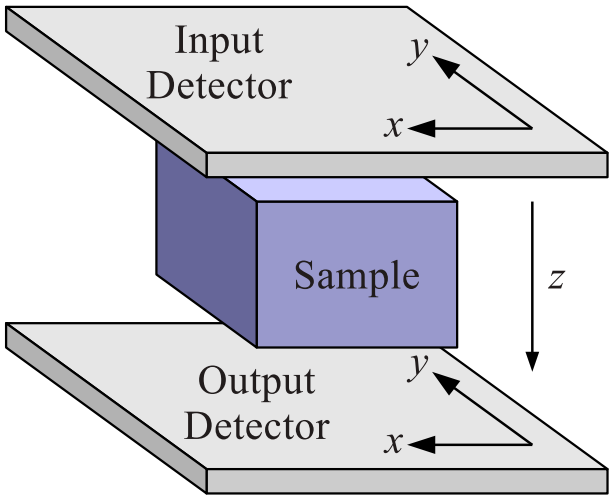

Figure 2: The Cartesian coordinate system used in equation 21.

The x and y basis vectors are defined to lie along the detector planes, while the z vector points from one plane to another. Therefore, the muon path can be represented using the functions $x(z)$ and $y(z)$ which, assuming that the muons don't double back on themselves, are single valued. The curvature in this form is given, as shown in A, by

$$\kappa^2\left(x(z), y(z)\right) = \frac{\left(\frac{\mathrm{d}^2x}{\mathrm{d}z^2}\right)^2 + \left(\frac{\mathrm{d}^2y}{\mathrm{d}z^2}\right)^2 + \left(\frac{\mathrm{d}x}{\mathrm{d}z}\frac{\mathrm{d}^2y}{\mathrm{d}z^2} - \frac{\mathrm{d}y}{\mathrm{d}z}\frac{\mathrm{d}^2x}{\mathrm{d}z^2}\right)^2}{\left(1 + \left(\frac{\mathrm{d}x}{\mathrm{d}z}\right)^2 + \left(\frac{\mathrm{d}y}{\mathrm{d}z}\right)^2\right)^3} \tag{18}$$

By Pythagoras's theorem, the infinitesimal element in l is related to those in the Cartesian coordinates x, y and z by

$$(\mathrm{d}l)^2 = (\mathrm{d}x)^2 + (\mathrm{d}y)^2 + (\mathrm{d}z)^2 \tag{19}$$

and so

$$\mathrm{d}l = \sqrt{1 + \left(\frac{\mathrm{d}x}{\mathrm{d}z}\right)^2 + \left(\frac{\mathrm{d}y}{\mathrm{d}z}\right)^2}\,\mathrm{d}z \tag{20}$$

Substituting these in gives

$$P = \exp\left[-\int_{z_{\mathrm{start}}}^{z_{\mathrm{end}}} \frac{1}{4D\left(x(z), y(z), z\right)} \frac{\left(\frac{\mathrm{d}^2x}{\mathrm{d}z^2}\right)^2 + \left(\frac{\mathrm{d}^2y}{\mathrm{d}z^2}\right)^2 + \left(\frac{\mathrm{d}x}{\mathrm{d}z}\frac{\mathrm{d}^2y}{\mathrm{d}z^2} - \frac{\mathrm{d}y}{\mathrm{d}z}\frac{\mathrm{d}^2x}{\mathrm{d}z^2}\right)^2}{\left(1 + \left(\frac{\mathrm{d}x}{\mathrm{d}z}\right)^2 + \left(\frac{\mathrm{d}y}{\mathrm{d}z}\right)^2\right)^{\frac{5}{2}}}\,\mathrm{d}z - \alpha\right] \tag{21}$$

The exponential function increases monotonically, and so to maximize it, only its argument is important. Therefore, by representing the probability as $P = \exp(-A - \alpha)$, the most probable path is that which minimizes the functional

$$A = \int_{z_{\text{start}}}^{z_{\text{end}}} \frac{1}{4D\left(x\left(z\right), y\left(z\right), z\right)} \frac{\left(\frac{\mathrm{d}^2 x}{\mathrm{d}z^2}\right)^2 + \left(\frac{\mathrm{d}^2 y}{\mathrm{d}z^2}\right)^2 + \left(\frac{\mathrm{d}x}{\mathrm{d}z}\frac{\mathrm{d}^2 y}{\mathrm{d}z^2} - \frac{\mathrm{d}y}{\mathrm{d}z}\frac{\mathrm{d}^2 x}{\mathrm{d}z^2}\right)^2}{\left(1 + \left(\frac{\mathrm{d}x}{\mathrm{d}z}\right)^2 + \left(\frac{\mathrm{d}y}{\mathrm{d}z}\right)^2\right)^{\frac{5}{2}}} \mathrm{d}z \tag{22}$$

which is an integral of curvature along the muon path. This formulation of the problem is useful, as by suitably constraining the minimization, the most probable path for a given set of detector measurements can be calculated. By constraining x and y at both ends of the integral, the entry and exit points can be specified. Similarly, by constraining $\mathrm{d}x/\mathrm{d}z$ and $\mathrm{d}y/\mathrm{d}z$ at both ends of the integral, the entry and exit angles can be specified.

3 Numerical method

The minima of the curvature functionals were calculated by discretizing the paths along the z axis, thus reducing the minimization to a finite-dimensional algebraic problem. (Another possible approach is to use the Calculus of Variations to convert the minimization problem to an equality problem. The corresponding Euler Lagrange equations, however, are a coupled pair of third-order nonlinear partial differential equations, which would be more difficult to solve.)

The first step is to represent the z-axis using N discrete points, in which case $2N$ numbers are required to describe the curve. Of these, the start and end points are fixed by the boundary conditions, and so there are in fact $2N - 4$ arguments of minimization. The angles of entry and exit are specified by fixing $\mathrm{d}x/\mathrm{d}z$ and $\mathrm{d}y/\mathrm{d}z$ at the start and end points. At all other points, the 1st derivatives can be calculated using a three-point stencil as

$$\frac{\mathrm{d}x}{\mathrm{d}z} \rightarrow \frac{x_{n+1} - x_{n-1}}{2\delta z} \tag{23}$$

$$\frac{\mathrm{d}y}{\mathrm{d}z} \rightarrow \frac{y_{n+1} - y_{n-1}}{2\delta z} \tag{24}$$

Similarly, the 2nd derivatives can be calculated as

$$\frac{\mathrm{d}^2 x}{\mathrm{d}z^2} \rightarrow \frac{x_{n+1} - 2x_n + x_{n-1}}{\left(\delta z\right)^2} \tag{25}$$

$$\frac{\mathrm{d}^2 y}{\mathrm{d}z^2} \rightarrow \frac{y_{n+1} - 2y_n + y_{n-1}}{\left(\delta z\right)^2} \tag{26}$$

where at the start and end points, the stencil uses fixed pre-start and post-end points, as calculated by extrapolating the start and end points using the $\mathrm{d}x/\mathrm{d}z$ and $\mathrm{d}y/\mathrm{d}z$ boundary conditions. These pre-start and post-end points are not just a way of solving array edge problems; they are in fact a crucial part of the method, as they force the solution to comply with the first-derivative boundary conditions. Without this technique, the resulting solution would be a straight line connecting the entry and exit points, with a sharp kink at either end. Using the technique, such pathological kinks would add a very high value to the functional, thus suppressing them.

In this discretized form, the functional becomes

$$A\left(x_1 \ldots x_N, y_1 \ldots y_N\right) = \tag{27}$$

$$\sum_{n=1}^{N} \frac{\left(\frac{x_{n+1} - 2x_n + x_{n-1}}{(\delta z)^2}\right)^2 + \left(\frac{y_{n+1} - 2y_n + y_{n-1}}{(\delta z)^2}\right)^2 + \left(\frac{x_{n+1} - x_{n-1}}{2\delta z}\frac{y_{n+1} - 2y_n + y_{n-1}}{(\delta z)^2} - \frac{y_{n+1} - y_{n-1}}{2\delta z}\frac{x_{n+1} - 2x_n + x_{n-1}}{(\delta z)^2}\right)^2}{4D\left(x_n, y_n, z_n\right)\left(1 + \left(\frac{x_{n+1} - x_{n-1}}{2\delta z}\right)^2 + \left(\frac{y_{n+1} - y_{n-1}}{2\delta z}\right)^2\right)^{5/2}} \delta z$$

The resulting $2N - 4$ dimensional minimization problem does not necessarily have the solution approximating the original continuum problem as its only minimum. Furthermore, there is no obvious

reason to believe that the desired minimum will even be the lowest minimum. Therefore, it is necessary to initialize the minimization technique with a curve that has the same basic form of the anticipated solution, and complies with the boundary conditions. The chosen initialization was

$$x_{\mathrm{i}}(z) = x_1 + x_2 \frac{z - z_{\mathrm{start}}}{z_{\mathrm{end}} - z_{\mathrm{start}}} + x_3 \sin\left(\pi \frac{z - z_{\mathrm{start}}}{z_{\mathrm{end}} - z_{\mathrm{start}}}\right) + x_4 \sin\left(2\pi \frac{z - z_{\mathrm{start}}}{z_{\mathrm{end}} - z_{\mathrm{start}}}\right) \quad (28)$$

$$y_{\mathrm{i}}(z) = y_1 + y_2 \frac{z - z_{\mathrm{start}}}{z_{\mathrm{end}} - z_{\mathrm{start}}} + y_3 \sin\left(\pi \frac{z - z_{\mathrm{start}}}{z_{\mathrm{end}} - z_{\mathrm{start}}}\right) + y_4 \sin\left(2\pi \frac{z - z_{\mathrm{start}}}{z_{\mathrm{end}} - z_{\mathrm{start}}}\right) \quad (29)$$

The coefficients x_1 and y_1 specify the entry point. The coefficients x_2 and y_2 specify the exit point. The coefficients x_3, x_4, y_3 and y_4, which only affect the starting and ending derivatives, are then used to fix the entry and exit angles.

The minimization was implemented in MATLAB, using code based around the "fminsearch" function. This uses the Nelder-Mead minimization method.

4 Results

Calculations of most probable muon trajectory were done for a variety of input and output conditions. In all cases a planar object was assumed to lie halfway between the detectors, the profile of which is given in Figure 3. The functional form of the object, in terms of the scattering coefficient D, is

$$\frac{1}{D(z)} = 1 - \left(1 - \frac{1}{\eta}\right) \mathrm{sech}\left(10\left(z - \frac{1}{2}\right)\right) \quad (30)$$

where the coefficient η specifies the ratio in D between the center of the object, and the background medium. This choice of function is not particularly important; it is just a simple way of implementing a smoothly varying planar structure.

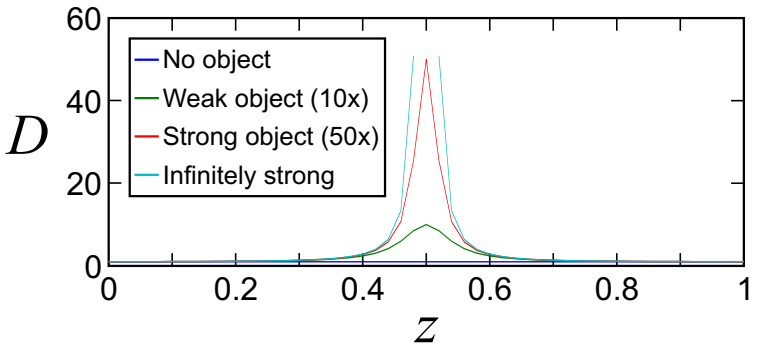

Figure 3: Profile of the scattering coefficient D, of the planar object used in the muon path calculation, along the z axis.

Multiple calculations were performed, for different scattering coefficients relative to the surrounding medium. For clarity, exaggerated scattering angles are used. Figure 4 shows the result for muons with intersecting input and output trajectories. Figure 5 shows the result for muons with nonintersecting input and output trajectories. Figure 6 shows the result for muons with parallel input and output trajectories, in which case the POCA path (unless detector errors are assumed) becomes ill defined.

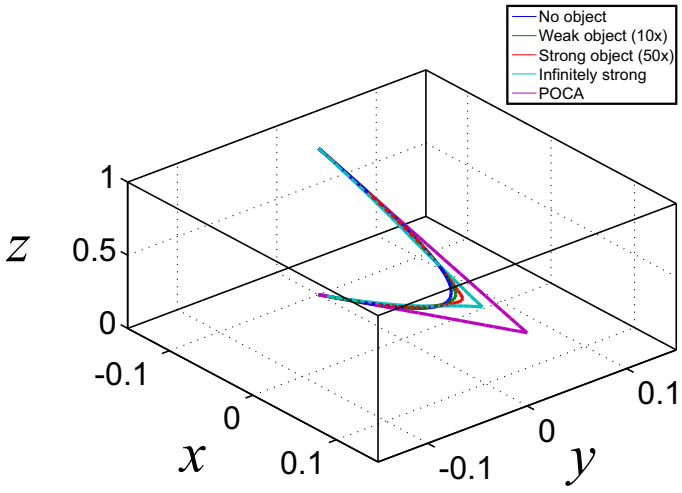

Figure 4: Most probable paths for intersecting input and output trajectories.

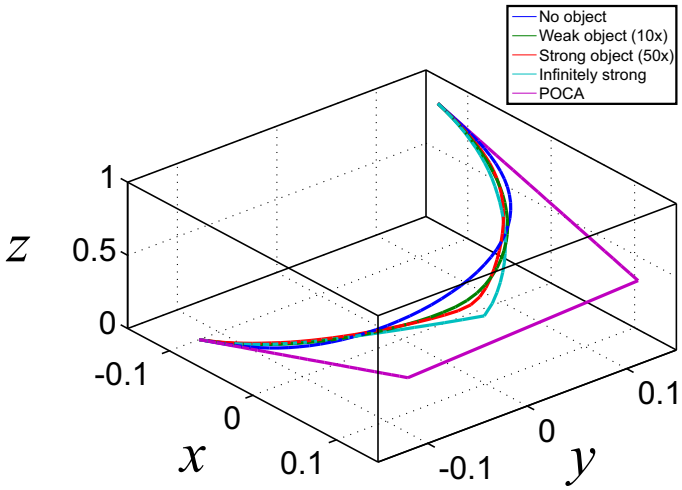

Figure 5: Most probable paths for nonintersecting input and output trajectories. In such a case, the POCA method must either assume that the detector measurements are inaccurate, or (as shown) that there is a sudden jump between the input and output trajectories.

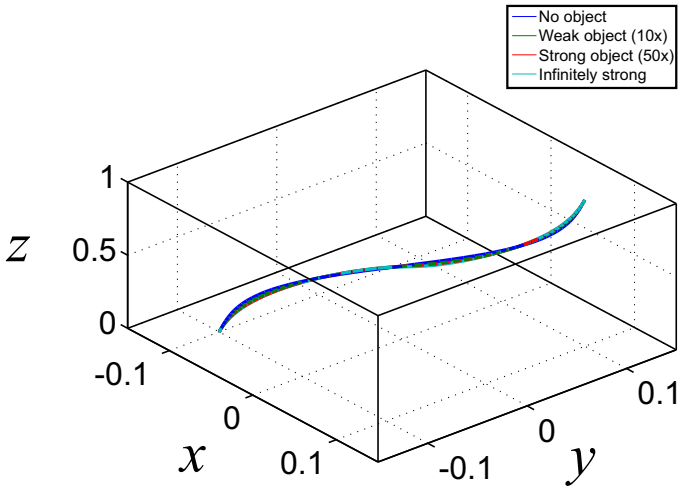

Figure 6: Most probable paths for parallel input and output trajectories.

5 Conclusions

A method to calculate the most probable muon trajectory through a scattering medium, for given input and output trajectories has been developed. Firstly, the problem of maximizing probability was reformulated as a problem of minimizing a functional describing the integrated curvature of the muon path. Secondly, an algorithm for finding the muon path which minimizes the functional was developed. The method returns trajectories that are sometimes similar to, but don't match POCA trajectories. Unlike POCA, the integrated curvature path calculation is compatible with any prior assumption as to the distribution of scattering materials, and can naturally handle cases where the extrapolated input and output trajectories fail to intersect.

There are several possibilities for future research. One route is to introduce more physics into the diffusion calculation. For example, the scattering PDF varies from the Gaussian distribution of the current model at high scattering angles [10, 11], which ideally should be accounted for. We are also planning to make speed optimizations to the functional minimization algorithm, to accommodate the very large numbers of path computations that would be required for any practical application. These computational requirements are discussed in B.

In the longer term, we aim to integrate the minimum curvature integral technique into tomographic reconstructions. A more accurate path model could allow for imaging with both higher spatial resolution and higher contrast. One such technique is to take the result from an initial reconstruction, use this to calculate more probable muon paths, and then perform a better reconstruction. It may be possible to extend this into an iterative scheme, in which successive improvements to the muon paths and to the resulting image converge upon an optimum solution.

The minimum curvature integral technique may also help in the analysis of errors in the muon detectors. At present, when determining the validly of muon measurements, there is always a compromise between rejecting real data, and allowing spurious information to enter the reconstruction. As the minimum curvature integral technique provides a probability value, this could be used as a prior probability in Bayesian analysis of the detector errors.

From a mathematical viewpoint, there is scope to develop a more rigorous method for extracting usable finite numbers from the infinitesimal probabilities that result from the diffusion calculation. A potential lead in this, is the similarity between the derivation and that of Feynman path integral techniques. These have been extensively studied in the field of quantum mechanics, and are used in many diffusion-like problems [12]. It is also possible that the very notion of taking a continuous limit is problematic, which in a physical sense may be justified, as the muons are ultimately undergoing a finite number of discrete scattering events.

A Curvature in Cartesian coordinates

A curved line in 3 dimensions, defined in cartesian coordinates as

$$\vec{r} = \begin{bmatrix} x(s) \\ y(s) \\ z(s) \end{bmatrix} \tag{31}$$

where x, y and z are functions of a parametric coordinate s, has curvature given by [13]

$$\kappa = \frac{\left| \frac{\mathrm{d}\vec{r}}{\mathrm{d}s} \times \frac{\mathrm{d}^2\vec{r}}{\mathrm{d}s^2} \right|}{\left| \frac{\mathrm{d}\vec{r}}{\mathrm{d}s} \right|^3} \tag{32}$$

By letting $s = z$, the first and second derivatives become

$$\frac{\mathrm{d}\vec{r}}{\mathrm{d}s} = \begin{bmatrix} \frac{\mathrm{d}x}{\mathrm{d}z} \\ \frac{\mathrm{d}y}{\mathrm{d}z} \\ 1 \end{bmatrix} \tag{33}$$

$$\frac{\mathrm{d}^2\vec{r}}{\mathrm{d}s^2} = \begin{bmatrix} \frac{\mathrm{d}^2x}{\mathrm{d}z^2} \\ \frac{\mathrm{d}^2y}{\mathrm{d}z^2} \\ 0 \end{bmatrix} \tag{34}$$

Substituting these into equation 32 gives

$$\kappa(x(z), y(z)) = \frac{\sqrt{\left(\frac{\mathrm{d}^2x}{\mathrm{d}z^2}\right)^2 + \left(\frac{\mathrm{d}^2y}{\mathrm{d}z^2}\right)^2 + \left(\frac{\mathrm{d}x}{\mathrm{d}z}\frac{\mathrm{d}^2y}{\mathrm{d}z^2} - \frac{\mathrm{d}y}{\mathrm{d}z}\frac{\mathrm{d}^2x}{\mathrm{d}z^2}\right)^2}}{\left(1 + \left(\frac{\mathrm{d}x}{\mathrm{d}z}\right)^2 + \left(\frac{\mathrm{d}y}{\mathrm{d}z}\right)^2\right)^{\frac{3}{2}}} \tag{35}$$

as required.

B Computational requirements

The curvature integral minimization technique is far more computationally demanding than POCA. From a numerical algorithms standpoint, the problem is that of unconstrained nonlinear optimization. There is no definitive algorithm for this type of problem, as the fastest method depends on both scale, and the computational cost of function evaluation. Assuming a z axis resolution of 1 cm, between detectors spaced about 3 m apart (which would accommodate a full size shipping crate), the minimization will have approximately $\mathcal{N} = 600$ parameters. In terms of computational complexity, this is a medium-scale problem, where the need for a low asymptotic growth order in the large $\mathcal{N}$ limit, must be balanced with small scale considerations, such as the magnitudes of proportionality coefficients.

A simple scheme is a Newton optimization method, for which the time consuming part is the Cholesky decomposition required to invert the Hessian matrix. This is at one extreme of the balance between asymptotic growth order and small-scale considerations. The growth order is unfavorable at $\mathcal{O}\left(\mathcal{N}^3\right)$, whereas the coefficient by which $\mathcal{N}^3$ is multiplied to give the required number of floating point operations is very favorable, at about 1/3. This makes the total requirement for a single iteration about 72 Mflop. The Hessian matrix would also account for the bulk of the data storage requirements. Assuming 8 bytes per value, a 600 × 600 symmetric matrix will occupy about 1.4 MB of memory. This is less than the cache per core of many modern processors, allowing each path calculation to proceed without the need to access external memory, and so allowing each core to run at close to peak efficiency.

The method also has the advantage of converging very rapidly, especially when given a good starting estimate. A practical implementation would probably provide these starting estimates from a database of precalculated paths. There are 8 degrees of freedom, due to the 4 parameters of both the input and output trajectories. However, for a homogeneous medium, there is a rotational symmetry around the z

axis and translational symmetries along the x and y axes, reducing this to 5 independent parameters. The size of the database can be greatly reduced by excluding paths above a certain deflection angle, and instead calculating such paths on the fly. Assuming 100 values are used for the first parameter, and 10 values are used for each of the subsequent restricted parameters, then the database will contain 1,000,000 paths. Assuming 8 bytes are needed for each of the 600 values within a path, the database will require 4.5 GB of storage space, which can easily be cached in RAM.

Given such a database, a typical path calculation will simply be a correction for interpolation error. This will probably take just a single iteration. If the path calculations are used in a recursive scheme (where the scattering densities from one set of path calculations are used to calculate a more realistic set of paths), then perhaps 5 iterations would be required for the most significant next step, with single iterations required for 4 subsequent refinement steps. The method would then require 720 Mflops per path.

This analysis only concerns one particular algorithm. An analysis of all rival algorithms is beyond the scope of this appendix. We present this special case, however, because it provides a rough upper bound to the computational requirement per muon.

Assuming a detector area of 30 m^2 (again, to accommodate a full size shipping crate) and a muon flux density of 1 cm^{-2} min^{-1}, then the muon flux will be 5000 s^{-1}. A sensible target for computation time, is that the total calculation takes no longer than the observation time, and so the minimization procedure must be repeated 5000 times per second. Combining this with the above estimate gives a total requirement of 3.6 Tflop/s.

These computational requirements are fairly demanding, but they must be seen in context. The cost of a muon tomographic device capable of accommodating an entire shipping crate is likely to be very high, and so the cost of the computer hardware will not be disproportionate. Furthermore, any application requiring real-time imaging is likely to be several years away, during which the necessary hardware will have become more easily obtainable. The problem is also highly parallelizable, allowing the computer to be used efficiently.

Acknowledgements

We received funding from The Atomic Weapons Establishment (AWE), under contract number 30182146.

References

References

[1] C. Morris, C. Alexander, J. Bacon, K. Borozdin, D. Clark, R. Chartrand, C. Espinoza, A. Fraser, M. Galassi, J. Green, J. Gonzales, J. Gomez, N. Hengartner, G. Hogan, A. Klimenko, M. Makela, P. McGaughey, J. Medina, F. Pazuchanics, W. Priedhorsky, J. Ramsey, A. Saunders, R. Schirato, L. Schultz, M. Sossong, G. Blanpied, Tomographic Imaging with Cosmic Ray Muons, Science & Global Security 16 (1) (2008) 37–53.

[2] M. Alamaniotis, S. Terril, J. Perry, R. Gao, L. Tsoukalas, T. Jevremonic, A mutilsignal detection of hazardous materials for homeland security, Nuclear Technology & Radiation Protection 1 (2009) 46–55.

[3] W. Gilboy, P. Jenneson, S. Simons, S. Stanley, D. Rhodes, Muon radiography of large industrial structures, Nuclear Instruments and Methods in Physics Research B 263 (2007) 317–319.

[4] H. Tanaka, T. Nakano, S. Takahashi, J. Yoshida, K. Niwa, Development of an emulsion imaging system for cosmic-ray muon radiography to explore the internal structure of a volcano, mt. asama, Nuclear Instruments and Methods in Physics Research Section A: Accelerators, Spectrometers, Detectors and Associated Equipment 575 (2007) 489–497.

[5] N. Lesparre, D. Gilbert, J. Marteau, Y. Declais, D. Carbone, E. Galichet, Geophysical muon imaging: feasibility and limits, Geophysical Journal International 183 (2010) 1348–1361.

[6] L. Schultz, K. Borozdin, J. Gomez, G. Hogan, J. McGill, C. Morris, W. Priedhorsky, A. Saunders, M. Teasdale, Image reconstruction and material Z discrimination via cosmic ray muon radiography, Nuclear Instruments and Methods in Physics Research Section A: Accelerators, Spectrometers, Detectors and Associated Equipment 519 (2004) 687–694.

[7] L. Schultz, G. Blanpied, K. Borozdin, A. Fraser, N. Hengartner, A. Klimenko, C. Morris, C. Orum, M. Sossong, Statistical Reconstruction for Cosmic Ray Muon Tomography, IEEE Transactions on Image Processing 16 (8) (2007) 1985–1993.

[8] S. Pesente, S. Vanini, M. Benettoni, G. Bonomi, P. Calvini, P. Checchia, E. Conti, F. Gonella, G. Nebbia, S. Squarcia, G. Viesti, A. Zenoni, G. Zumerle, First results on material identification and imaging with a large-volume muon tomography prototype, Nuclear Instruments and Methods in Physics Research A 604 (2009) 738–746.

[9] D. Williams, The most likely path of an energetic charged particle through a uniform medium, Physics in Medicine and Biology 49 (2004) 2899–2911.

[10] A. Butkevich, R. Kokoulin, G. Matushko, S. Mikheyev, Comments on multiple scattering of high-energy muons in thick layers, Nuclear Instruments and Methods in Physics Research A 488 (2002) 282–294.

[11] G. Wang, L. Schultz, J. Qi, Statistical Image Reconstruction for Muon Tomography Using a Gaussian Scale Mixture Model, IEEE Transactions on Nuclear Science 56 (4) (2009) 2480–2486.

[12] G. W. Johnson, M. L. Lapidus, The Feynman integral and Feynman's operational calculus, Oxford Science Publications, 2002.

[13] E. Kreyszig, Differential Geometry, Dover Books on Mathematics, 1996.